Optogenetic investigation of cardiac arrhythmia mechanisms

Feola, I.

Chapter 6

OPTOGENETICALLY-INDUCED MICROFOCI OF OXIDATIVE STRESS INCREASE PROARRHYTHMIC RISK

Iolanda Feola*, MSc; Wanchana Jangsangthong*, PhD;
Alexander Teplenin*, MSc; Martin J. Schalij, MD, PhD;
Dirk L. Ypey, PhD; Antoine A.F. de Vries, PhD; Daniël A. Pijnappels, PhD

Laboratory of Experimental Cardiology, Department of Cardiology, Heart Lung Center Leiden; Leiden University Medical Center, the Netherlands.
*equal contribution

In preparation for submission

ABSTRACT

Introduction

Coronary microvascular dysfunction (CMD) is associated with oxidative stress (OS) and cardiac arrhythmias. However, the mechanisms of these arrhythmias remain obscure. We hypothesized that microfoci of excessive reactive oxygen species (ROS) production lead to local electrophysiological disturbances, thereby increasing pro-arrhythmic risk. To test this hypothesis, we used a unique combination of optogenetics and patterned illumination to precisely control ROS production in time and space.

Methods and results

Neonatal rat ventricular cardiomyocytes (NRVCs) were cultured and transduced with either lentiviral vectors encoding a plasma membrane-bound version of a photo-inducible ROS-generating protein (RGP) called miniSOG or control green fluorescence protein (GFP). ROS generation was induced by 470 nm light irradiation. The effects of ROS on cardiac electrophysiology were evaluated at single-cell and monolayer level. Upon irradiation, ROS levels were significantly increased in NRVCs expressing miniSOG (NRVC-miniSOG). Patch-clamp recordings showed that irradiation-induced changes in electrical activity of NRVC-miniSOG-PM in a time-dependent manner, like depolarization of resting membrane potential, early afterdepolarizations, and sustained depolarization. Optical voltage mapping of NRVC-miniSOG monolayers following irradiation of 0.75-6mm in diameter, circular areas revealed diameter- and time-dependent pro-arrhythmic effects ranging from AP prolongation, conduction slowing to functional conduction block with triggered activity. Importantly, electrical pacing of irradiated NRVC-miniSOG monolayers resulted in tachyarrhythmias sustained by a reentrant circuit anchored to the ROS-induced functional conduction block in 15 out of 60 cultures. None of these effects were observed in control cultures.

Conclusion

This is the first study to reveal a pro-arrhythmic role for microfoci of oxidative stress. Such microfoci lead to disturbances in electrical impulse generation and propagation, thereby enabling formation of reentrant tachyarrhythmias, and providing novel insight into the role of oxidative stress in arrhythmias.

Keywords

Regional oxidative stress, optogenetics, arrhythmias, reentry, optical mapping, patch-clamp.

INTRODUCTION

Coronary microvascular dysfunction (CMD) is characterized by structural[1] or functional[2] alterations of the inner wall of the coronary pre-arterioles and arterioles that can lead to spasms and decreased blood flow to the heart muscle.[3,4] Such dysfunction might, therefore, be associated with patchily distributed myocardial ischemia[5] and consequently with oxidative stress (OS), *i.e.* an overproduction of reactive oxygen species (ROS).[6,7] Indeed, during an ischemic event, the mitochondria increase the ROS production because of a positive feedback called "ROS-induced ROS release".[8] Furthermore, several studies have shown that an additional ROS burst is mainly correlated with the blood reperfusion of the ischemic area.[9-14] Although it is well known that ROS can give rise to electrophysiological alterations and therefore increase the risk of arrhythmia onset, the pathophysiological progression of such alterations in time and space remain poorly understood due to the lack of dedicated research tools. Indeed, thus far the regional ROS overproduction has been challenging to achieve as well as the investigation of its effects on cardiac electrophysiological properties. In this study, we used a photo-inducible ROS-generating protein (RGP),[15]called miniSOG (mini singlet oxygen generator),[16] and patterned illumination to spatially and temporally control ROS production, by blue-light illumination. Furthermore, miniSOG was targeted to the plasma membrane (PM) of neonatal rat ventricular cardiomyocytes (NRVC) to mimic the ROS release in the vicinity of cardiac ion channels/transporters. Such approach allowed us to investigate whether and how local OS could affect the electrophysiological properties of cardiac cells and thereby induce cardiac arrhythmias.

MATERIALS AND METHODS

An expanded Methods section is provided in the Supplemental Material.

In the present study, NRVCs were isolated, cultured and transduced with either lentiviral vectors encoding miniSOG-PM or eGFP-PM (Figure 1A). At day 2-4 post-transduction, ROS overproduction was induced by blue-light (470 nm) illumination and evaluated by fluorescent microscopy imaging, while its effects were investigated via patch-clamp recording and optical-voltage mapping experiments.

RESULTS

Light-induced oxidative stress in miniSOG-PM-NRVCs

ROS generation in NRVCs was assessed by using fluorescent imaging. As shown in Figure 1B and 1C, under normal growth conditions, the ROS level was not different in non-transduced NRVCs (control) and NRVCs expressing miniSOG-PM (miniSOG-PM) and eGFP-PM (eGFP-PM).

To examine whether blue light could contribute to ROS overproduction, miniSOG-PM-NRVCs, eGFP-PM-NRVCs, and control-NRVCs were exposed to blue light for 4 min. Following such illumination, only miniSOG-PM-NRVCs showed significantly increased in ROS production ($P<0.001$) (Figure 1D and 1E). No significant changes were observed in eGFP-PM-NRVCs and control-NRVCs.

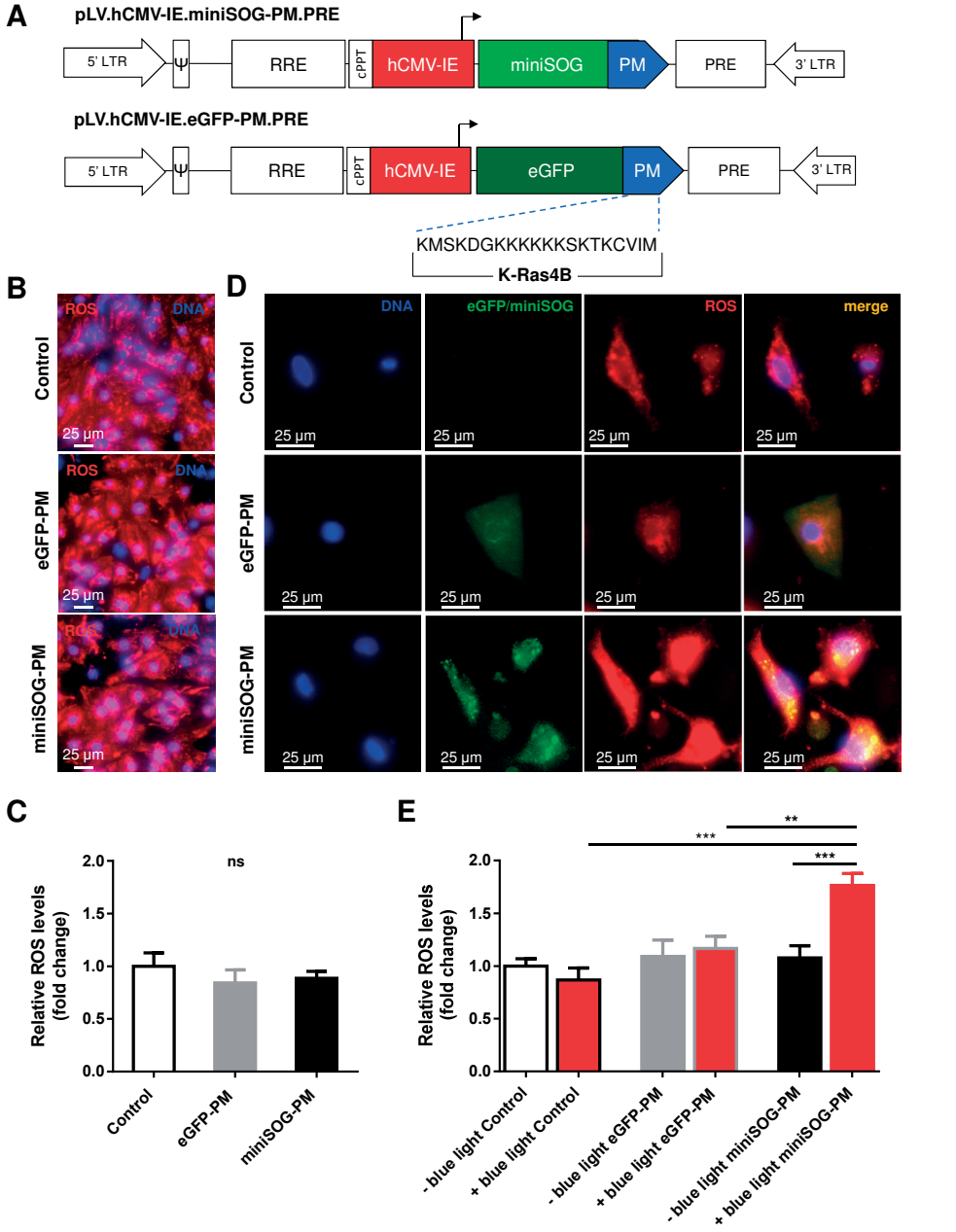

Figure 1. Lentiviral constructs and fluorescence microscopy of NRVCs. A, Proviral DNA structure of LV.miniSOG-PM (top) and LV.eGFP-PM (bottom) showing plasma membrane (PM) targeting domain that contains a C-terminal polybasic sequences of the K-Ras4B. The different abbreviations are explained in the paragraph designated 'Plasmid construction and self-inactivating lentiviral vector (SIN-LV) production' of the Supplementary material. B, Live-cell fluorescent images of a non-transduced NRVC monolayer (top, control), a LV.eGFP-PM-transduced NRVC monolayer (middle, eGFP-PM), and a LV.miniSOG-PM-transduced NRVC monolayer (bottom, miniSOG-PM) in the absence of 470-nm light. Cells were stained ▸

for nuclei (DNA; blue) and reactive oxygen species (ROS; red). Scale bar: 25 μm. C, Quantitative analysis of ROS levels detected in monolayers were assessed from red fluorescent signal. Bars show ROS level under normal growth condition (control, white, n=4; eGFP-PM, gray, n=6; miniSOG-PM, black, n=5). D, Live-cell fluorescent images were captured immediately following exposure to 470-nm light for 4 minutes from non-transduced NRVCs (top, control), eGFP-PM-NRVCs (middle, eGFP-PM) and miniSOG-PM-NRVCs (bottom, miniSOG-PM). These cells were stained for nuclei (DNA, blue) and ROS (red) using Hoechst 33342 and CellRox Deep Red reagent, respectively. Scale bar: 25 μm. E, Quantitative analysis of ROS levels detected in cells were assessed from red fluorescent signal. Bar graphs show basis ROS level under normal growth conditions (control, white, n=12; eGFP-PM, gray, n=11; miniSOG-PM, black, n=11). Corresponding filled red bars show ROS level following 470-nm light irradiation (control, n=10; eGFP-PM, n=7; miniSOG-PM, n=16). **P<0.01 and ***P<0.001.

Electrophysiological characterization of miniSOG-PM-NRVCs

The baseline electrophysiological parameters of miniSOG-PM-NRVCs and eGFP-PM-NRVCs were characterized. First, perforated and whole-cell patch-clamp techniques were used to characterize such parameters in single NRVCs. Figure 2A shows action potentials (APs) recorded in the absence of blue light from a miniSOG-PM-NRVC (black trace) and a eGFP-PM-NRVC (gray trace). Both showed similar spontaneous activity, which is typical of NRVCs.[17] Analysis of mean peak (Figure 2B) and mean steady-state (Figure 2C) total current-voltage (I-V) relationships reveals no difference between miniSOG-PM-NRVCs and eGFP-PM-NRVCs. These results indicate that such genetic manipulation did not change the electrophysiological properties of NRVCs under normal growth conditions.[18]

Next, optical-voltage mapping was performed to characterize the electrophysiological properties of eGFP-PM-NRVC and miniSOG-PM-NRVC monolayers. Upon 1-Hz electrical point stimulation, both eGFP-PM-NRVC and miniSOG-PM-NRVC monolayers showed uniform and convex APs propagation from the bipolar pacing electrode (Figure 2H).

No significant differences of action potential duration (APD) and conduction velocity (CV) were observed between eGFP-PM-NRVC and miniSOG-PM-NRVC monolayers; APD_{30} was 128±9 ms vs 142±9 ms (P=0.28), APD_{50} was 165±12 ms vs 186±13 ms (P=0.24), APD_{80} was 276±19 ms vs 275±16 ms (P=0.96), and CV was 19±0.4 cm/s vs 18±0.6 cm/s (P=0.31). (Figure 2D-G and 2I).

Effect of regional oxidative stress in miniSOG-PM-NRVC monolayers

To evoke regional ROS overproduction in NRVC monolayers, a circular pattern (6 mm diameter) of constant blue light (470nm, 0.3 mW/mm^2) was projected to the center of the monolayers for 2, 4 and 6 minutes (Figure 3A and 3B, left). The effects of ROS overproduction on electrophysiological properties were characterized during 1-Hz electrical stimulation. Figure 3B and the Supplementary Table I show that blue-light illumination did not significantly affect the electrical activity of eGFP-PM-NRVC monolayers. In contrast, obvious changes in electrical activity were observed in miniSOG-PM-NRVC monolayers upon blue-light illumination (Figure 3B-E). As shown in Figure 3C, following 2 minutes central illumination and 1-Hz electrical pacing of miniSOG-PM-NRVC monolayers, a significant prolongation in APD was

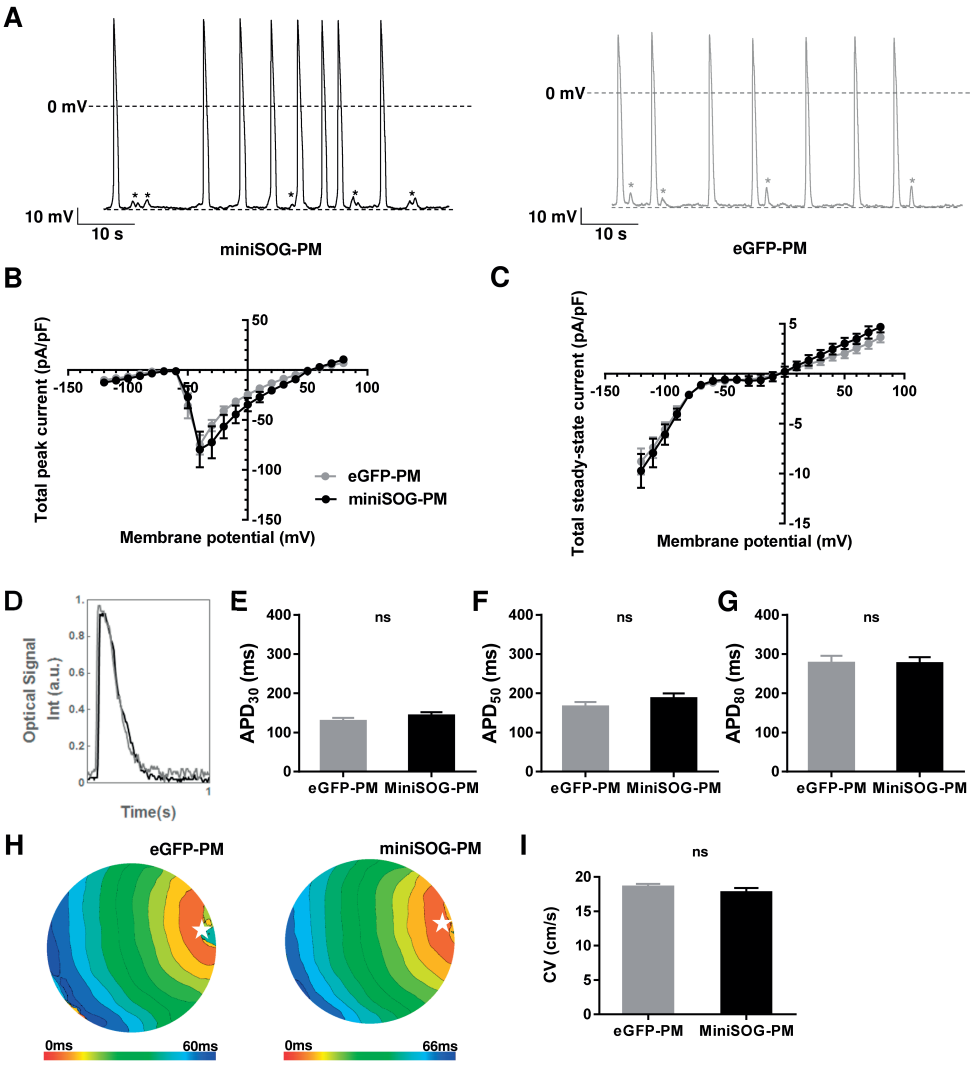

Figure 2. Characterization of single cells and 2-dimensional models of genetically engineered NRVCs. A, typical APs in a miniSOG-PM-NRVC (black) and an eGFP-PM-NRVC (gray). The recordings were obtained by perforated patch-clamp techniques. The voltage-current (I-V) curves of the peak (B) and steady-state (C) current density were expressed as the mean ± SEM and derived from miniSOG-PM-NRVCs (filled black circle; *n*=6) and eGFP-PM-NRVCs (filled grey circle; *n*=8). B, was obtained from the current amplitudes at the beginning of each voltage steps, and (C) was obtained from steady-state currents at the end of 400-ms test pulses. To record the total membrane currents, 400-ms voltage pulses between -130 and +70 mV were applied in 10 mV increments every 5 s from the holding potential of -90 mV. D, optical signal traces of LV.eGFP-PM-transduced (grey) and LV.miniSOG-PM-transduced (black) NRVC monolayer cultures paced at 1-Hz. Quantification APD_{30} (E), APD_{50} (F), and APD_{80} (G). H, Representative activation maps (6-ms isochrone spacing). I, Assessment of CV by optical-voltage mapping.

observed in the area exposed to blue light (the OS zone) when compared with non-exposed area (non-OS zone); APD_{30} was 161±11 ms vs 304±27 ms (P<0.001), APD_{50} was 188±15 ms vs 344±39 ms (P<0.05), and APD_{80} was 284±25 ms vs 438±50 ms. (P<0.05), n=13. When illumination time was extended to 4 minutes, the ultralong APD was observed in the OS zone of miniSOG-PM-NRVC monolayers during 1-Hz electrical pacing, and ectopic spontaneous activities were noted in 15 of 15 monolayers. As illustrated in Figure 3D, uniform propagation originating from the bipolar pacing electrode was observed during the first stimulus upon 1-Hz electrical pacing. Then, ectopic beats, which originated at a site of the border of the OS zone, initiated propagation, went outward and around the OS zone and terminated at the opposite side of their origin due to the collision of the wavefronts. Of note, the ectopic beats and 1-Hz electrical pacing stimuli were unable to propagate into the OS zone due to its sustained depolarization activity during 6 s data acquisition. Next, following illumination of miniSOG-PM-NRVC monolayers central area, we applied single electrical stimulus and continued monitoring of the depolarization duration of OS zone. Interestingly, we found a variation of the duration of ultralong APD (data not shown). When miniSOG-PM-NRVC monolayers were illuminated for 6 minutes, in addition to spontaneous ectopic activities found in 8 of 15 miniSOG-PM-NRVC monolayers, 7 of 15 of miniSOG-PM-NRVC monolayers exhibited conduction slow in the OS zone during 1-Hz electrical pacing. As shown in Figure 3E, decreased CV was observed in the OS zone. On average CV in the OS zone significantly decreased when comparing to the values before illumination (18±0.4 cm/s vs 8±0.4 cm/s [P<0.001]). In contrast, the average CV in the non-oxidative stress zone did not change following blue-light illumination (18±0.4 cm/s vs 18±0.3 cm/s [P=0.7]).

Additional experiments were conducted to estimate the minimum size of the OS zone needed to give rise to the ectopic phenomena previously described. Figure 4A shows photographs of miniSOG-PM-NRVC monolayers with 0.75-, 1.5- and 3-mm circular patterns of blue light in place.

Following illumination for 6 minutes, ectopic waves and ultra-long APD appeared and spread through the entire monolayer from the oxidative stress zone of 3- and 1.5-mm but not 0.75-mm, Figure 4A and B). Configuration rearrangement did not affect the initiation and propagation of ectopic waves (Figure 4A). Analysis of ectopic incident from 15 miniSOG-PM-NRVC monolayers confirmed that 3-mm circular pattern showed to be the most capable to give rise to spontaneous ectopic beats follow by 1.5-mm circular pattern, whereas the ectopic incident did not appear from 0.75-mm circular one (Figure 4C).

Effect of oxidative stress in single miniSOG-PM-NRVCs

Next, we performed perforated patch-clamp recordings to characterize the effect of OS on electrophysiological changes in single miniSOG-PM-NRVCs and eGFP-PM-NRVCs.

As shown in Figure 5A, which represents similar results from 5 other eGFP-PM-NRVCs, no changes in electrical activity were observed. In contrast, Figure 5B shows that irradiation of a miniSOG-PM-NRVC caused marked changes in electrical activity. We observed the occurrence of changes on second-time scale (14.61±5.28 s; *n*=9). The rapid progression of changes

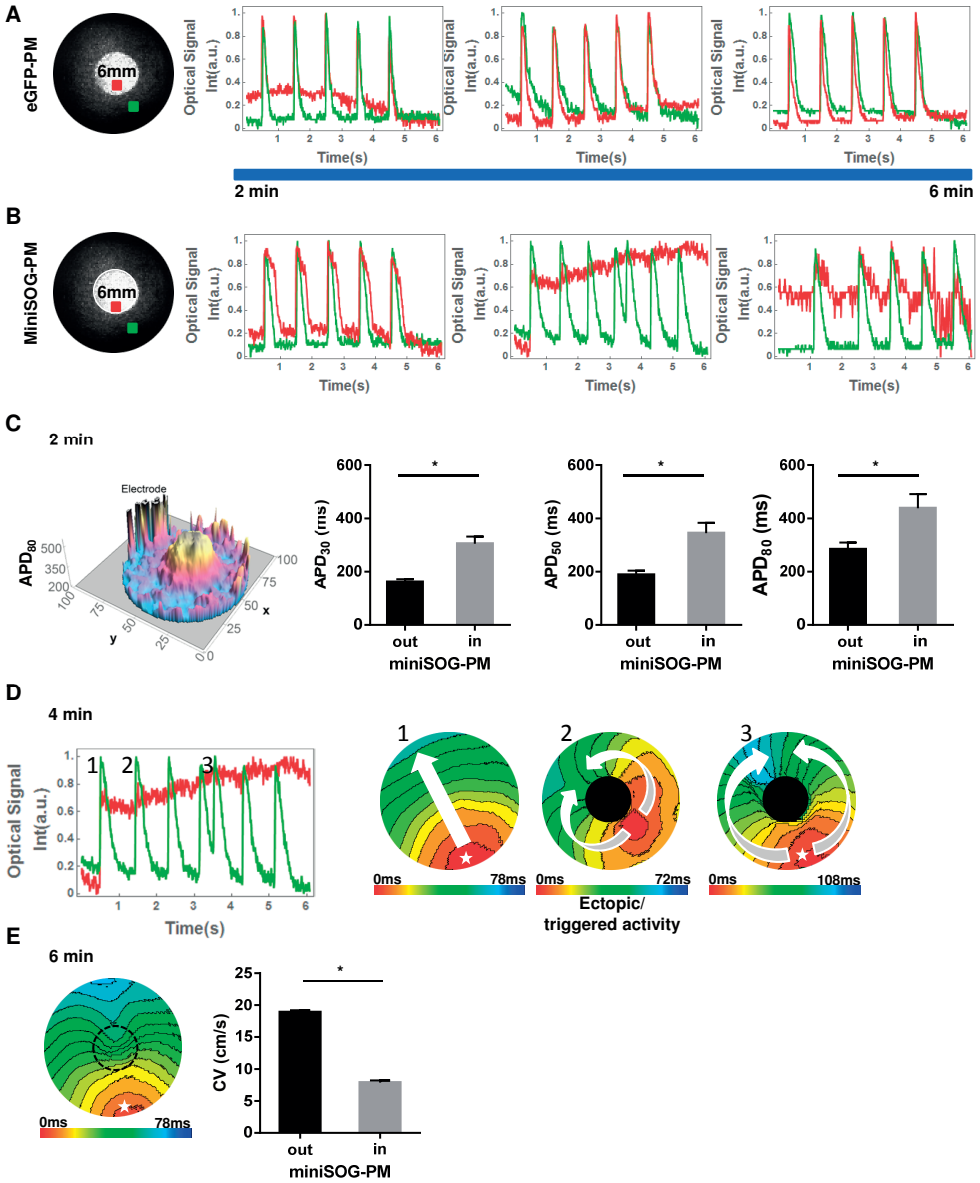

Figure 3. Regional elevated ROS production alters cardiac electrophysiology and leads to disturbances of electrical impulse generation and propagation. A and B, Screenshot of round NRVC monolayers (15-mm-diameter) (left) transduced with LV.eGFP-PM (A) and LV. miniSOG-PM (B), showing a circle and central area (6-mm diameter), which was exposed to 470-nm light. Optical traces (right) show light dosage-dependent effects on the electrical activity. Optical signal traces in green and red are representing non-irradiated and irradiated areas. C, 3-dimensional APD map shows the prolongation occurring only in the circular and central area exposed for 2 minutes to 470-nm light in the miniSOG-PM-NRVC monolayers (left). This map shows bell-shape like distribution of APD values inside OS zone, with the highest APD values in the center of the area. Comparison of APD_{30}, APD_{50}, APD_{80} between irradiated and non-irradiated areas (right). n=10, *P<*0.05*. D, Typical optical trace (left) showing the ultra-long APD and triggered beats ▸

occurring when miniSOG-PM-NRVC monolayers were electrically paced at 1Hz after 4 minutes 470-nm light exposure. The activation maps (right) are showing the uniform propagation of the electrical stimulus originating from the bipolar pacing electrode, the triggered ectopic beat originated at a site of the border of the OS zone, and a subsequent electrical stimulus that could be elicited but could not propagate in the OS zone due to the ultralong APD. D, Activation map (left) showing the conduction slowing occurring only in the irradiated area of miniSOG-PM-NRVC monolayers exposed to 470-nm light for 6 minutes (7 out 15). Comparison of CV between irradiated and non-irradiated area (right). (n=7), *P<*0.001*.

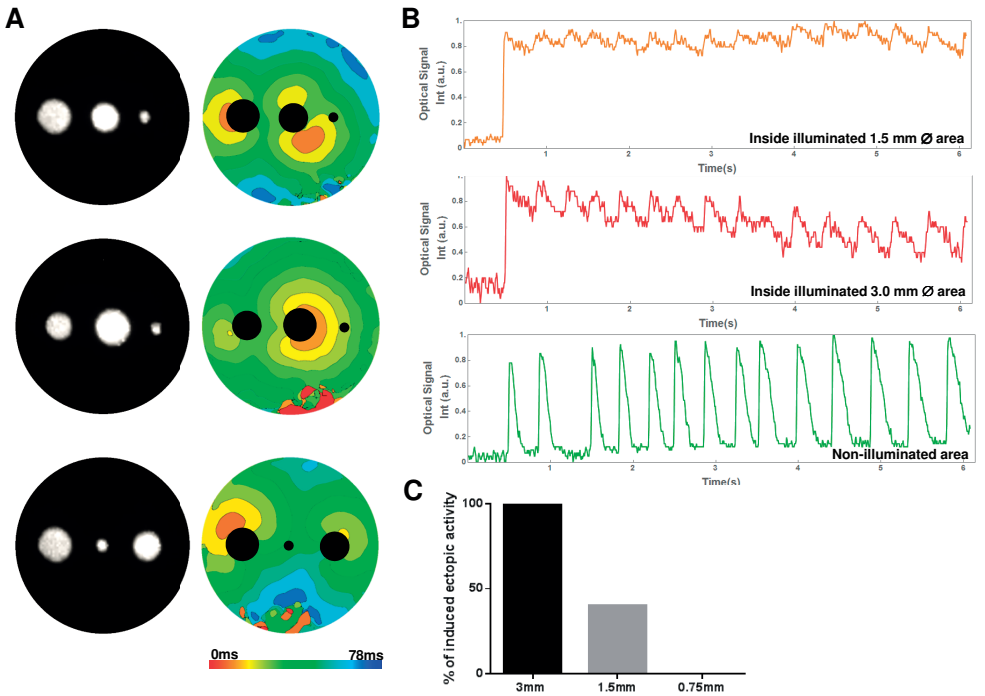

Figure 4. Size threshold of regional elevated ROS area for generation of ultralong APD and ectopic beats in miniSOG-PM-NRVC monolayers. A, Screenshot of round NRVC monolayers (15-mm-diameter) showing 3 circular areas under light exposure (3-1.5-0.75 mm diameter) arranged in 3 different configurations (left). B, The activation maps are showing that upon 6 minutes irradiation ectopic triggered beats could be originated only from the 3 and 1.5 mm size circular areas. C, Optical traces from non-irradiated (green) and irradiated areas, 3 mm in red and 1.5 mm in orange. Red and orange traces show the ultralong APD, the green trace shows ectopic beats. D, Comparison of the incidence of ectopic beats originating from the areas with different diameters.

consisted of an initial shift in membrane potential from -73.71±0.78 mV to -66.86±1.30 mV (*n*=9; P<0.001), the APD prolongation with the occurrence of early afterdepolarizations (EADs) (Figure 5B, a), and a sustained depolarization (Figure 5B, b). The sustained depolarization began with an AP that strongly depolarized the membrane potential. Then, membrane potential gradually declined on a timescale of minutes to a sustained depolarization between -30 and -10 mV. Similar results were obtained in other 8 miniSOG-PM-NRVCs. These findings suggested

a dose-dependent effect of ROS overproduction to cause a rapid, pronounced and dynamic alteration of electrical activities in response to irradiation time.

We hypothesized that the longer irradiation of miniSOG-PM-NRVC led to higher amount of ROS production and thereby progressively altering its electrical activity. To test this, we reduced the irradiation time to 10-s. Likewise, Figure 5C shows that brief irradiation of miniSOG-PM-NRVC was capable to markedly lengthen APD and caused the occurrence of EADs before spontaneous recovery of the resting membrane potential (RMP). After 4-5 minutes, AP shortening progressively appeared, as shown in Figure 5C, AP j. Moreover, following irradiation, a subsequent decline in AP amplitude and plateau potential were also observed (Figure 5C and 5D). Whereas, the depolarization of RMP and a sustained depolarization after an AP were not noticed. These findings were similar in 3 other miniSOG-PM-NRVCs.

To further characterize the dosage-dependent effects of ROS on AP alteration, we additionally performed whole-cell recordings in 3 miniSOG-PM-NRVCs.

As shown in Figures 5E, in comparison with the AP recorded in the absence of blue light (black trace), increased ROS overproduction corresponding to irradiation-time not only affected AP amplitude but also reduced AP upstroke velocity, which observed in short (10-s; red trace) and long (60-s; blue trace) irradiation. Moreover, long exposure to blue light caused depolarization of RMP. These results confirmed our findings from perforated-patch recordings and verified the dosage-dependent effect of an elevated ROS to alter cardiac electrical activities.

Since miniSOG is targeted to PM, locally ROS overproduction in the vicinity of cardiac ion channels/transporters can be assumed upon illumination of the miniSOG-PM-NRVCs. Therefore, a possible explanation for the electrophysiological changes could be directly implicated to the effect of ROS on cardiac ion channels/transporters. To investigate this, we performed whole-cell voltage-clamp recording before and after blue-light irradiation in miniSOG-PM-NRVCs to characterize the changes in membrane ionic current. As expected, when a miniSOG-PM-NRVCs was exposed to blue light, excessive ROS was generated and markedly modulated total membrane currents during the voltage-step recording (Supplementary Figure 1). Because the changes in electrical activity induced by ROS were dynamic and occurred very rapid, alterations in the magnitude of whole-cell currents may be expected. Therefore, a ramp protocol that required less time for data acquisition was designed to deliberate current produced by cell over the potentials between -130 mV and +50 mV and introduced to examine 4 miniSOG-PM-NRVCs in order to obtain a quasi-steady-state I-V relationship. This type of plots was used by Qu and Chung to explain the mechanisms underlying the roles of different ionic currents on APD lengthening and EAD genesis in a mathematical model of cardiac myocyte.[19] Figure 6A shows the representative quasi-steady-state currents recorded from a miniSOG-PM-NRVC before (black trace) and after 10-s (red trace) and 60-s (blue trace) blue-light irradiation. The circles in Figure 6A depict the quasi-equilibrium states, where the total outward currents equal to the total inward currents. The black one approximately at -70 mV is the resting potential. The gray and open circles show quasi-equilibrium states at the plateau voltage. In comparison with control (black trace), the quasi-equilibrium state at the plateau voltage is enlarged and occupied longer voltage length following 10-s blue-light irradiation (red trace).

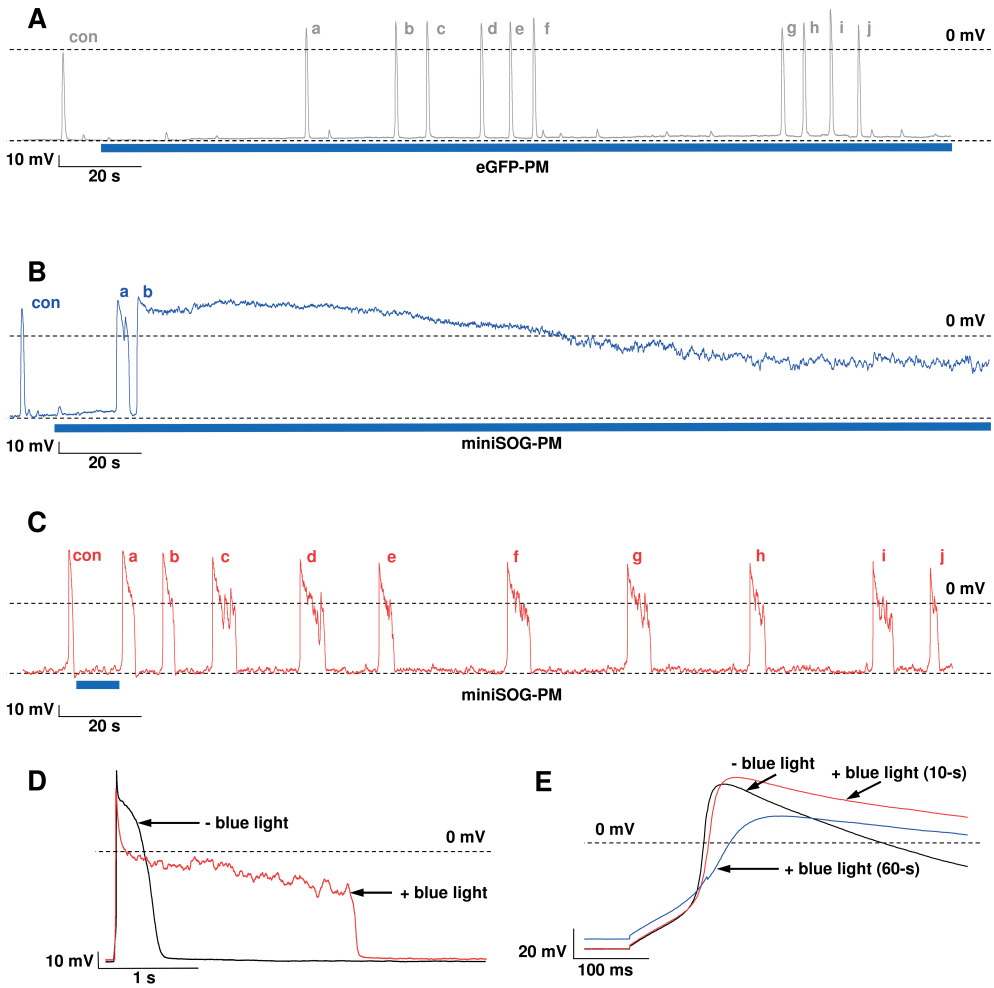

Figure 5. Effect of elevated ROS on the electrical activity of single spontaneous beating NRVCs. Perforated patch-clamp technique was employed to recode and monitor spontaneous electrical activity of NRVCs for ≥ 4 minutes. A, electrical activity of an eGFP-PM-NRVC (eGFP-PM) during continuous irradiation with 470-nm light. The typical action potentials (APs) are observed before (con) and after the start of continuous illumination (a-j). B, electrical activity of a miniSOG-PM-NRVC (miniSOG-PM) during continuous illumination with 470-nm light. The rapid progression from a normal AP (con) ranging from the slight resting membrane potential depolarization and lengthening AP duration (APD) with an early afterdepolarization (EAD) (a) to a failure to repolarization (b) are observed. C, electrical activity of a miniSOG-PM-NRVC following brief exposure (10-s) to 470-nm light. The following alterations in electrical activity were observed: in a and b, APD prolongation; in c-i, decline in AP amplitude, oscillation in plateau phase with the occurrence of EADs, and prolongation of APD; in j, APD shortening. D, the effect of ROS on AP amplitude and plateau potential and APD observed in a miniSOG-PM-NRVC. Black trace illustrates the AP recorded in the absence of 470-nm light, and red trace shows the AP recorded following 470-nm-light illumination. E, light dosage-dependent effects on reduction of AP upstroke velocity and amplitude. A miniSOG-PM-NRVC was stimulated by square current pulses (100-pA, 5-ms) to evoke the APs just before (control, black trace) and at two times after the start of 470-nm-light illumination; brief irradiation (10-s, red trace) and continuous irradiation (60-s, blue trace).

Suggesting that elevated ROS significantly alter the inward current, and this current can then act against the unchanged or slightly elevated outward currents to maintain the plateau phase of AP thereby leading to AP lengthening. Since voltage-dependent L-type Ca^{2+} channels ($Ca_V1.X$) play the main role to generate the inward current during the plateau, elevated ROS may have the effects on $Ca_V1.X$ gating and thus the window L-type Ca^{2+} current (I_{CaL}).

To examine whether the changes in membrane inward current carried mainly by I_{CaL} could be induced by elevated ROS, we performed voltage-clamp experiments in 5 miniSOG-PM-NRVCs using conventional step-type voltage-clamp protocols. We found that the alteration of the quasi-equilibrium states at the plateau was not only due to the change of I_{CaL} kinetics but also the increase of I_{CaL} (Figure 6B).

Furthermore, some specific changes in another inward current carried by mainly voltage-dependent Na^+ current (I_{Na}) including the alteration in peak current and inactivation kinetics (Figure 6C) were also observed following blue light irradiation. These findings suggest that the presence of late I_{Na} in combination with alteration of window I_{CaL} help the formation of the quasi-equilibrium states at the plateau voltage, which may be responsible for the underlying mechanism of elevated ROS causing ultralong APD and EADs. In addition, when OS was further increased by extending irradiation-time to 60 s, we observed the further alteration of the quasi-equilibrium states. As shown in Figure 6A, blue trace, the lower two quasi-equilibrium states disappear and the only equilibrium state for the upper plateau voltage remains. This indicates the loss of the equilibrium state for the resting potential thereby the membrane voltage cannot decrease to the physiological RMP due to the decline of mainly resting K^+ current (I_{K1}). Moreover, increase in outward current positive to -10 mV and negative shift in holding current were observed. Suggesting the presence of leak current, which favors a failure to repolarize after an AP thereby leading to a sustained depolarization around the remained quasi-equilibrium voltage.

Effect of regional oxidative stress on arrhythmias in miniSOG-PM-NRVC monolayers

Finally, we investigated the effect of the regional OS on arrhythmogenesis in miniSOG-PM-NRVC monolayers. Based on our finding described above, we employed paced beats that developed from the bipolar pacing electrode placed somewhere along the periphery of the monolayer to initiate reentry. Two different strategies to induce reentry, namely, "ectopic stimulation" and "burst pacing" were utilized.

As shown in Figure 7A (left) and 7C (left), for both reentry inducing approaches, first paced beat was capable to uniformly propagate through the entire monolayers. In line with the result as shown in Figure 5D, following first paced beat, sustained depolarization and extremely APD prolongation (2-24 s) were observed in the OS zone. Corresponding optical traces for OS zone (red) and non-OS zone (green) are shown in Figure 7B and 7D.

For ectopic stimulation approach as shown in Figure 7A (middle), we observed the propagation of ectopic beat as described in Figure 3D. Therefore, we applied a properly timed electrical paced beat to face the refractory tail of the ectopic beat leading to developing of

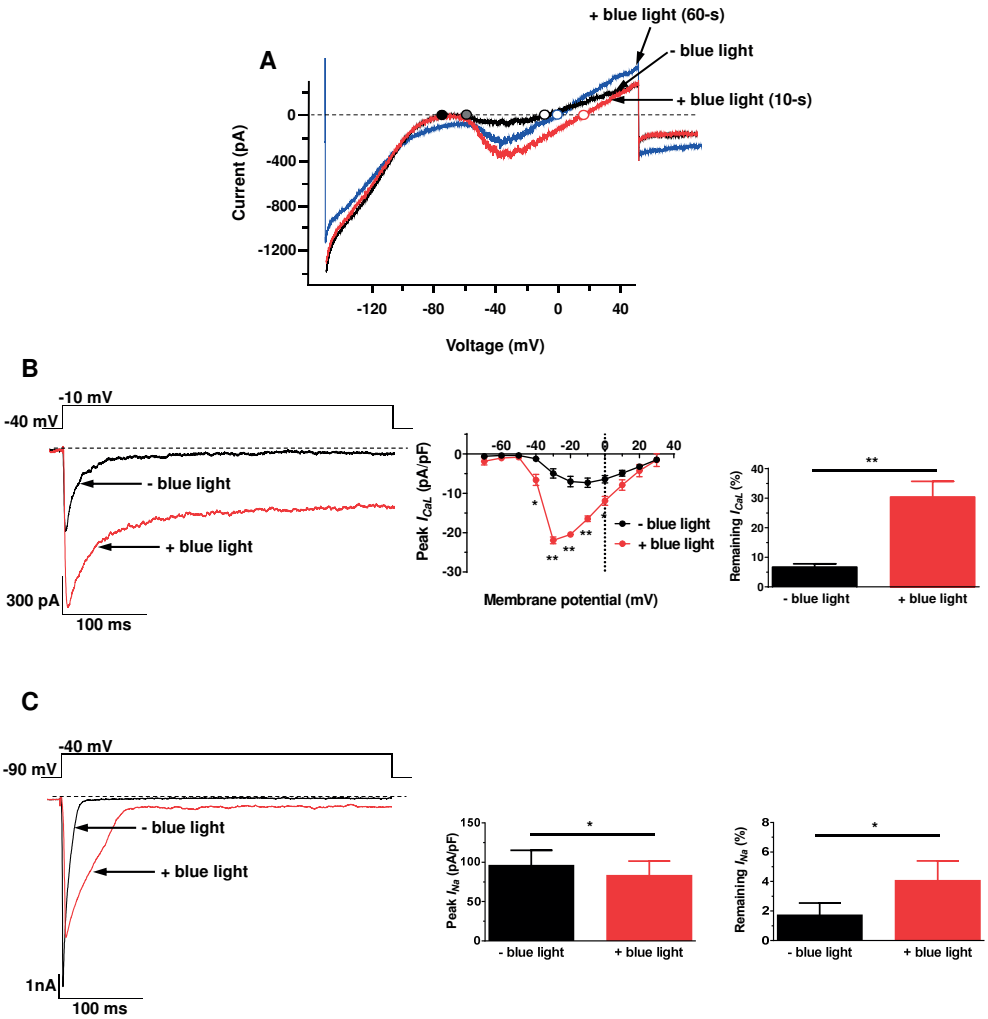

Figure 6. Effects of ROS on the quasi-equilibrium states and ionic currents of miniSOG-PM-NRVCs. A, the quasi-steady-state I-V curves of a miniSOG-PM-NRVC recorded before (black) and after 10-s (red) and 60-s (blue) blue-light illumination. These I-V curves were evoked by ramping membrane potential between -130 and +50 mV over 8 seconds from holding potential of -90 mV. B, Left: current traces representing mainly I_{CaL} recorded from the holding potential (V_h) = -40 mV stepped to -10 mV for 400-ms obtained before (black) and after 10-s (red) blue-light illumination. While performing this recording, I_{Na} I_{CaT} are inactivated by V_h. B, Middle: comparison of I-V curves of peak I_{CaL} derived before (black) and after 10-s (red) exposure to blue light, n=5. B, Right: quantitative analysis of remaining I_{CaL} at 350-ms derived before (black) and after 10 s (red) blue- light illumination, n=5. C, Left: current traces representing mainly I_{Na} elicited by stepping to -40 mV from a V_h of -90 mV for 400-ms obtained before (black) and after 10-s (red) 470-nm-light illumination. C, Middle: quantitative analysis of maximum peak I_{Na} density derived before (black) and after 10-s (red) exposure to blue light, n=5. C, Right: quantitative analysis of remaining I_{Na} at 350-ms derived before (black) and after 10 s (red) blue-light illumination, n=5 . *P<0.05 and **P<0.01.

uni-directional conduction block, which resulted in the initiation of a ring-like reentrant wave rotating around the OS region (Figure 7A [right]).

For burst pacing approach, following first paced beat, we electrically paced the highest possible frequency that led to 1:1 capture (Figure 7A, middle). Thereby, initiation of ectopic beat was not observed. However, continued high-frequency electrical pacing developed a uni-directional conduction block and successfully induced ring type reentry (Figure 7C [right] a).

As shown in Figure 7E, we induced and observed stable reentry (lasting ≥ 6 s) in 6 out of 30 and 9 out of 30 miniSOG-PM transduced NRVC monolayers by means of ectopic stimulation and burst pacing stimulation, respectively. In addition, we also induced and observed unstable

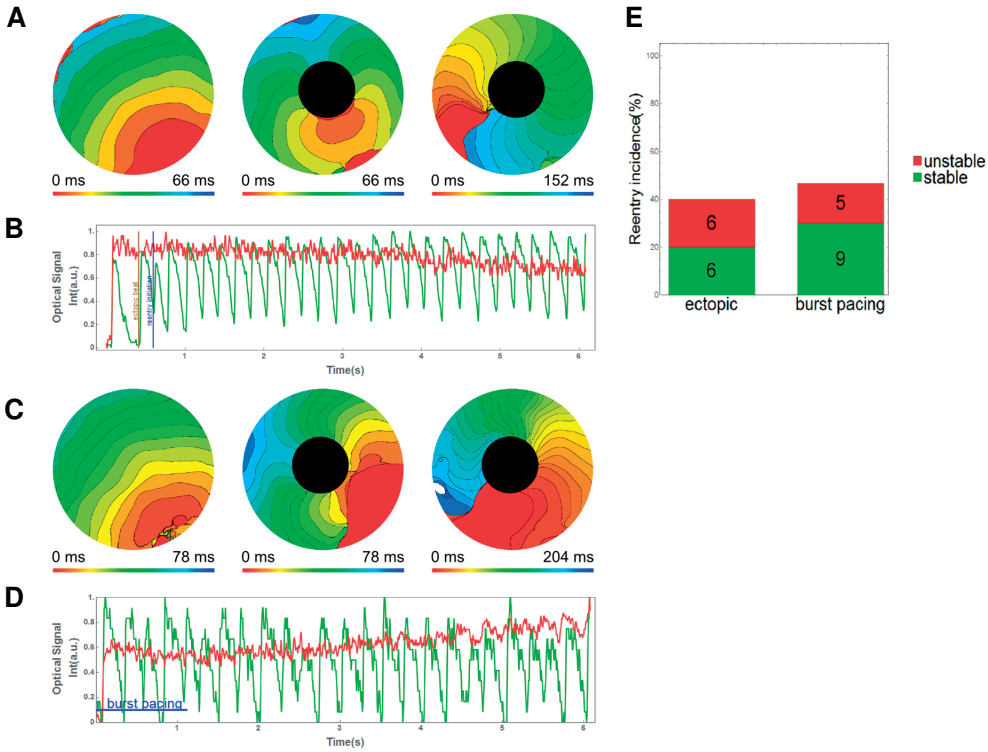

Figure 7. Regional elevated ROS production causes reentry arrhythmias in miniSOG-PM-NRVC monolayers. A and B, Activation maps (A) and optical traces (B) showing the 'ectopic beat' protocol employed to in induce ring-like reentrant wave rotating around the OS region. After the first electrical stimulus and the consequent triggered ectopic beat, a second electrical stimulus was applied. The proper timing allowed to face the refractory tail of the ectopic beat leading to uni-directional conduction block and reentry establishment. C and D, Activation maps (C) and optical traces (D) showing the 'burst pacing' protocol employed to in induce ring-like reentrant wave rotating around the OS region. After the first electrical stimulus monolayers were electrically paced at the highest possible frequency that led to 1:1 capture, uni-directional conduction block, and reentry establishment. E, Quantification of stable and unstable reentry initiation for both type of protocols.

or self-terminating reentry episodes (lasting for 2-4 s): 6 for ectopic stimulation and 5 for burst pacing (Figure 7E).

DISCUSSION

Coronary microvascular dysfunction (CMD) is characterized by abnormalities in the coronary blood flow that can lead to myocardial ischemia and therefore to oxidative stress (OS).[6,7] Such ischemic events are localized in small myocardial areas, *i.e.* patchily distributed in the myocardium.[5] Furthermore, since those little foci are surrounded by myocardial tissue that is normally functioning, CMD is very difficult to be detected and investigated. In the present study, a photo-inducible ROS-generating protein (RGP),[15] called miniSOG,[16] was used in combination with patterned illumination to create localized areas of OS and investigate whether and how those areas could induce electrophysiological alterations and thereby increase proarrhythmic risk. One of our main motivations to study the effect of local OS was to improve our understanding of its role in cardiac arrhythmias, in a way that was not possible before.

In our study, optical-voltage mapping and patch-clamp experiments showed that the exposure of miniSOG-PM-NRVC cultures to blue light led to an increased intracellular ROS level that caused electrophysiological changes in a dose-dependent manner.

At single-cell level, we found that increased OS depolarized the membrane, depressed AP amplitude, lengthened APD, caused oscillation in the membrane potential during the plateau, EADs, and repolarization failure. In monolayers, we observed time- and diameter-dependent pro-arrhythmic effects of the OS area ranging from electrophysiological changes (APD lengthening, slowed conduction) to arrhythmogenic consequences (functional conduction block, ectopic beats, reentry). Those alterations have been also described in other studies, where different experimental models were used.[20-26] However, our approach allowed us to localize OS in areas of different dimensions, which could not be achieved, for instance, by means of global administration of primary ROS or ROS-generating reagents (*e.g.* potassium superoxide, hydrogen peroxide (H_2O_2) and xanthine/xanthine oxidase).

The main ROS in cardiac myocytes exists of free radical species, such as superoxide anion ($O_2^{\cdot -}$) and hydroxyl radical ($^{\cdot}OH$), or of nonradical species, such as H_2O_2, $^1O_2$ and nitrogen species.[27] MiniSOG generates $^1O_2$ which is an oxygen molecule with an unpaired electron at the higher orbital. Such property makes $^1O_2$ highly reactive and believed to be one of the most damaging species. Furthermore, it is characterized by limited diffusion and lack of selectivity. Because of the aforementioned characteristics, $^1O_2$ is capable to react in the immediate vicinity of its generation. Moreover, since $^1O_2$ is generated by lipid peroxidation of the plasma membrane via other ROS,[28, 29] in this study, miniSOG was targeted to the cardiac cell membrane to mimic $^1O_2$ natural localization, *i.e.* in the vicinity of cardiac ion channels/transporters. Based on this approach, we can attribute the observed electrophysiological alterations to ROS-induced modification of cardiac ion channels. However, we cannot rule out the effects of ROS on a dramatic increase in intracellular Ca^{2+} $[Ca^{2+}]_i$ by an increased diastolic Ca^{2+} leak through enhanced ryanodine receptor (RyR2) open probability, which leads together with dysfunctional

sarcoplasmic reticulum (SR) Ca^{2+} ATPase (SERCA2a) to reduced SR Ca^{2+} load. This coupled with an influx of Ca^{2+} through the damaged sarcolemma would cause an increase in free $[Ca^{2+}]_i$ which can, in turn, initiate arrhythmias.[27,30,31] Indeed, our optical mapping of $[Ca^{2+}]_i$ showed that the $[Ca^{2+}]_i$ transient was dramatically prolonged following exposure of miniSOG-PM-NRVC monolayers to blue light due to ROS overproduction (Supplementary Figure 2).

MiniSOG has been originally employed in cell ablation experiments because of its toxic effects.[16, 32] To avoid such permanent damage we chose durations of irradiation that led to sub-lethal ROS generation and allowed us to reveal a dose-dependent effect of ROS on cardiac electrophysiological alterations and arrhythmias.

On the basis of single-cell experiments, we found that the electrophysiological alterations might involve specific changes in membrane ionic currents, *i.e.* I_{K1}, I_{Na}, I_{CaL} and nonselective cation current (I_{NSC}). The alterations, such as the positive shift in RMP of ≥ 5 mV and the lengthening in AP duration, might be due to a reduction in resting K^+ current through I_{K1} (Figure 6A, blue trace), which may indicate a decrease in the channel open probability under OS.[33,34] Furthermore, alterations in amplitude, plateau and repolarization phases of an AP may involve changes in I_{Na}, I_{CaL} ,and I_{NSC}, which have been already described to be affected by OS.[35] It has been reported that Na^+ channel oxidation not only causes a gradual reduction in I_{Na}, but also results in a slowing of inactivation referred as a late I_{Na} component.[27, 36] Therefore, ROS-enhanced late I_{Na} could contribute to the accumulation of intracellular Na^+, AP prolongation, EADs, and arrhythmias. [20,30, 36] Although redox modification of $Ca_V1.X$ modulation still remains a matter of debate since ROS can result both in increased and decreased I_{CaL}, depending on the type, level and location of ROS generation,[30] our findings likely replicate redox modifications that lead to an increased in I_{CaL}. This suggests that ROS overproduction can alter biophysical properties of I_{CaL}, resulting in significant alteration of the quasi-equilibrium states at the plateau, thereby promoting AP lengthening and EADs occurrence.[19] These EADs were characterized by oscillations with increasing amplitude towards the end of the AP (Figure 5C). Such increase in amplitude is similar to the observation by Song *et al*, who linked this phenomenon to Ca^{2+} overload, increased I_{CaL} and the leakage of RyR2.[37] In our study, we cannot rule out the possibility that stress kinases, like cAMP-dependent protein kinase A (PKA), protein kinase C (PKC), and Ca^{2+}/calmodulin-dependent protein kinase II (CaMKII), can activate both I_{Na} and I_{CaL} by phosphorylation, because all three kinases are subject to ROS-dependent oxidation/activation.[20,32, 33] The sustained depolarization resulted from ROS may be attributed to the activation of $I_{NSC.}$ The activation of this leak current, would be expected to cause a concomitant decline in AP amplitude, plateau potential and delayed repolarization, as observed in Figure 5D. Therefore, given the consequences of ROS-induced electrical alteration following blue light irradiation, we presume that severe activation of I_{NSC} would add to repolarization failure as demonstrated in Figure 5B.

At the monolayers level, we show that miniSOG-PM-NRVC monolayers were characterized by abnormalities in the generation and/or propagation of electrical impulses when regional OS was generated by patterned blue-light illumination.

We show that perturbed AP propagation in miniSOG-PM-NRVC monolayer occurs when the OS zone exhibits extremely APD lengthening or conduction slowing. Here, APD

lengthening is characterized by a quasi-stable depolarized state, lasting from 2 to 24 seconds (data not shown). This is in line with the incidence of ultralong APD and EADs observed at single-cell level. Therefore, the presence of ultralong APD in the OS zone in miniSOG-PM-NRVC monolayer may act as a functional disturbance of cardiac electric impulse propagation (functional conduction block) during sinus rhythm. The slow conduction observed here could be also explained with single-cell data, *i.e.* significant reduction in I_{Na} peak current and shift in RMP. In addition, ROS might play a role in gap junction dysfunction. Indeed, during regional OS, ROS may affect the balance of stress kinases and phosphatases in a way that favors the dephosphorylation of connexin 43 (Cx43), which would result in a decrease in gap junctional conductance, thereby contributing to persistent CV slowing in the OS zone.

Disturbance in AP generation, as shown here, were characterized by abnormal automaticity (ectopic beats) arising from the OS border zone of miniSOG-PM-NRVC monolayers. The regionally confined OS zone was characterized by APD prolongation and EADs, which might depolarize the neighboring cardiomyocytes, localized in the non-OS zone, giving rise to triggered activity. The phenomenon of heterogeneity of APD causing ectopic activity has been described in atrial myocytes by Nattel *et al.*[38]

In conclusion, this study revealed that microfoci of OS lead to disturbances in both electrical impulse generation (*i.e.* EADs, ectopic beats) and propagation (*i.e.* functional conduction block and slowing), thereby favoring reentrant arrhythmia formation. These results provide novel insight into the role of microsubstrates in arrhythmogenesis, which are substrates still left undetectable, and therefore untreated if present, in the current clinical setting.

ACKNOWLEDGMENTS

We thank Cindy Bart (Department of Cardiology, LUMC) for assistance with the animal experiments and Annemarie Kip (Department of Cardiology, LUMC) for LV production.

SOURCES OF FUNDING

This work was supported by the Netherlands Organisation for Scientific Research (NWO, Vidi grant 91714336 to D.A.P.). Additional support was provided by Ammodo (D.A.P. and A.A.F.d.V.).

DISCLOSURES

None.

REFERENCES

1. Opherk D, Zebe H, Weihe E, Mall G, Durr C, Gravert B, Mehmel HC, Schwarz F, Kubler W. Reduced coronary dilator capacity and ultrastructural changes of the myocardium in patients with angina pectoris but normal coronary arteriograms. Circulation. 1981; 63:817– 825.
2. Richardson PJ, Livesley B, Oram S, Olsen EG, Armstrong P. Angina pectoris with normal coronary arteries: transvenous myocardial biopsy in diagnosis. Lancet. 1974; 2:677– 680.
3. Camici PG, d'Amati G, Rimoldi O. Coronary microvascular dysfunction: Mechanisms and functional assessment. Nat.Rev.Cardiol. 2015; 12:48-62.
4. Anderson RD, Pepine CJ. The coronary microcirculation in stemi: The next frontier? Eur.Heart J. 2015; 36:3178-3181.
5. Maseri A, Crea F, Kaski JC, Crake T. Mechanisms of angina pectoris in syndrome X. J Am Coll Cardiol. 1991; 17:499 –506.
6. Giordano FJ. Oxygen, oxidative stress, hypoxia and heart failure. J Clin Invest. 2005; 115:500–508.
7. Lucchesi BR. Free radicals and tissue injury. Dialogues Cardiovasc Med. 1998; 3:3–22.
8. Zorov DB, Filburn CR, Klotz LO, Zweier JL, Sollott SJ. Reactive oxygen species (ROS)-induced ROS release: a new phenomenon accompanying induction of the mitochondrial permeability transition in cardiac myocytes. J Exp Med. 2000; 192:1001–1014.
9. Hess ML, Manson NH. Molecular oxygen: friend and foe. The role of the oxygen free radical system in the calcium paradox, the oxygen paradox and ischemia/reperfusion injury. J Mol Cell Cardiol. 1984; 16:969–85.
10. Park JL, Lucchesi BR. Mechanisms of myocardial reperfusion injury. Ann Thorac Surg 1999; 68:1905–12.
11. Kilgore KS. Luchessi B.R. Reperfusion injury after myocardial infarction: the role of free radicals and the inflammatory response. Clin. Biochem. 1993; 359 370.
12. Zughaib ME, Tang XL, Sun JZ, Bolli R. Myocardial reperfusion injury: fact or myth? A 1993 appraisal of a seemingly endless controversy Ann. New York Acad. Sci. 1994; 723:218 228.
13. Ambrosio G, Tritto I. Reperfusion injury: experimental evidence and clinical implications Am. Heart J. 1999; 138:S69-S75.
14. Weisfeldt ML, Zweier J, Ambrosio G, Becker LC, Flaherty JT. Evidence that free radicals result in reperfusion injury in heart muscle. Basic Life Sci. 1988; 49:911-919.
15. Wojtovich AP, Foster TH. Optogenetic control of ros production. Redox.Biol. 2014;2:368-376.
16. Shu X, Lev-Ram V, Deerinck TJ, Qi Y, Ramko EB, Davidson MW, Jin Y, Ellisman MH, Tsien RY. A genetically encoded tag for correlated light and electron microscopy of intact cells, tissues, and organisms. PLoS.Biol. 2011; 9:e1001041.
17. Boink GJ, Verkerk AO, van Amersfoorth SC, Tasseron SJ, van der Rijt R, Bakker D, Linnenbank AC, van der Meulen J, de Bakker JM, Seppen J, Tan HL. Engineering physiologically controlled pacemaker cells with lentiviral hcn4 gene transfer. J.Gene Med. 2008; 10:487-497.
18. Engels MC, Askar SF, Jangsangthong W, Bingen BO, Feola I, Liu J, Majumder R, Versteegh MI, Braun J, Klautz RJ, Ypey DL, De Vries AA, Pijnappels DA. Forced fusion of human ventricular scar cells with cardiomyocytes suppresses arrhythmogenicity in a co-culture model. Cardiovasc.Res. 2015; 107:601-612.
19. Qu Z, Chung D. Mechanisms and determinants of ultralong action potential duration and slow rate-dependence in cardiac myocytes. PLoS One. 2012; 7:e43587.
20. Ward CA, Giles WR. Ionic mechanism of the effects of hydrogen peroxide in rat ventricular myocytes. The Journal of Physiology. 1997; 500:631.

21. Jabr RI, Cole WC. Alterations in electrical activity and membrane currents induced by intracellular oxygen-derived free radical stress in guinea pig ventricular myocytes. Circulation research. 1993; 72:1229-1244.

22. Jabr RI, Cole WC. Oxygen-derived free radical stress activates nonselective cation current in guinea pig ventricular myocytes role of sulfhydryl groups. Circulation research. 1995; 76:812-824.

23. Tarr M, Valenzeno DP. Modification of cardiac action potential by photosensitizer-generated reactive oxygen. Journal of molecular and cellular cardiology. 1989; 21:539-543.

24. De Diego C, Pai RK, Chen F, Xie L-H, De Leeuw J, Weiss JN, Valderrábano M. Electrophysiological consequences of acute regional ischemia/reperfusion in neonatal rat ventricular myocyte monolayers. Circulation. 2008; 118:2330-2337.

25. Kozhevnikov D, Caref EB, El-Sherif N. Mechanisms of enhanced arrhythmogenicity of regional ischemia in the hypertrophied heart. Heart rhythm : the official journal of the Heart Rhythm Society. 2009; 6:522-527.

26. Janse MJ, Van Capelle F, Morsink H, Kléber AG, Wilms-Schopman F, Cardinal R, d'Alnoncourt CN, Durrer D. Flow of" injury" current and patterns of excitation during early ventricular arrhythmias in acute regional myocardial ischemia in isolated porcine and canine hearts. Evidence for two different arrhythmogenic mechanisms. Circulation Research. 1980; 47:151-165.

27. Yang KC, Kyle JW, Makielski JC, Dudley SC, Jr. Mechanisms of sudden cardiac death: Oxidants and metabolism. Circ.Res. 2015; 116:1937-1955.

28. Miyamoto S, Martinez GR, Medeiros MH, Di MP. Singlet molecular oxygen generated by biological hydroperoxides. J.Photochem. Photobiol.B. 2014; 139:24-33.

29. Ambrosio G, Flaherty JT, Duilio C, Tritto I, Santoro G, Elia PP, Condorelli M, Chiariello M. Oxygen radicals generated at reflow induce peroxidation of membrane lipids in reperfused hearts. J. Clin. Invest. 1991; 87:2056-2066.

30. Wagner S, Rokita AG, Anderson ME, Maier LS. Redox regulation of sodium and calcium handling. Antioxid. Redox. Signal. 2013; 18:1063-1077.

31. Kohler AC, Sag CM, Maier LS. Reactive oxygen species and excitation-contraction coupling in the context of cardiac pathology. J.Mol.Cell Cardiol. 2014; 73:92-102.

32. Qi YB, Garren EJ, Shu X, Tsien RY, Jin Y. Photo-inducible cell ablation in caenorhabditis elegans using the genetically encoded singlet oxygen generating protein minisog. Proc. Natl. Acad. Sci. U.S.A. 2012; 109:7499-7504.

33. Nakaya H, Takeda Y, Tohse N, Kanno M. Mechanism of the membrane depolarization induced by oxidative stress in guinea-pig ventricular cells. J.Mol.Cell Cardiol. 1992; 24:523-534.

34. Shimoni Y, Clark RB, Giles WR. Role of an inwardly rectifying potassium current in rabbit ventricular action potential. J.Physiol. 1992; 448:709-727.

35. Carmeliet E. Cardiac ionic currents and acute ischemia: From channels to arrhythmias. Physiol Rev. 1999; 79:917-1017.

36. Jeong EM, Liu M, Sturdy M, Gao G, Varghese ST, Sovari AA, Dudley SC, Jr. Metabolic stress, reactive oxygen species, and arrhythmia. J. Mol. Cell Cardiol. 2012; 52:454-463.

37. Song Z, Ko CY, Nivala M, Weiss JN, Qu Z. Calcium-voltage coupling in the genesis of early and delayed afterdepolarizations in cardiac myocytes. Biophysical journal. 2015; 108:1908-1921.

38. Nattel S. New ideas about atrial fibrillation 50 years on. Nature. 2002; 415:219-226.

SUPPLEMENTAL MATERIAL

Detailed Methods

Neonatal Rat Ventricular Myocytes (NRVCs) Isolation and Culture

Animal protocols were reviewed and approved by the Animal Experiments Committee of the Leiden University Medical Center (LUMC) and conformed to the Guide for the Care and Use of Laboratory Animals as stated by the US National Institutes of Health. NRVCs were isolated from hearts of 2-day-old Wistar rat pups as previously described.[1, 2] Isolated cells were plated on round glass coverslips (15-mm diameter, Thermo Fisher Scientific Gerhard Menzel B.V. & Co. KG, Braunschweig, Germany) coating with fibronectin (Sigma-Aldrich, St. Louis, MO, USA) in 24-well plates (Corning Life Sciences, Amsterdam, the Netherlands). Depending on the assay, cell densities of 0.1-8 x 10^5 cells/well were used. To prevent perforation of non-cardiomyocytes, 12-16 hours after plating, cultures were treated for 2 hours with mitomycin-C (10 μg/mL; Sigma-Aldrich) as described previously.[2]

Plasmid Construction and Self-Inactivating Lentiviral Vector (SIN-LV) Production

SIN-LV shuttle plasmid pLV.hCMV-IE.miniSOG-PM.hHBVPRE, which codes for a plasma membrane-associated version of mini singlet oxygen generator (miniSOG), was constructed by a two-step procedure. In step 1, the miniSOG-coding sequence was extended with the plasma membrane targeting motif of human K-Ras4B by replacing the BglII×EcoRI fragment of plasmid miniSOG-C1 (Addgene, Cambridge, MA, USA, plasmid number: 54821)[3] with a linker molecule composed of oligonucleotides 5' GATCCAAGATGAGCAAAGACGGC AAAAAGAAGAAAAAGAAGTCCAAGACAAAGTGCGTGATCATGTAAAG 3' and 5' AATTCTTTACATGATCACGCACTTTGTCTTGGACTTCTTTTTCTTCTTTTT GCCGTCTTTGCTCATCTTG 3' (Sigma-Aldrich). The resulting plasmid was designated pminiSOG-PM. In step 2, the 414-bp Eco47III×EcoRI fragment of pminiSOG-PM was blunt-ended with Klenow polymerase and inserted in between the SmaI site and filled-in BsrGI site of pLV.hCMV-IE.IRES.eGFP.hHVBPRE.[1]

SIN-LV shuttle construct pLV.hCMV-IE.eGFP-PM.WHVoPRE encodes for a version of the *Aequorea victoria* enhanced green fluorescent protein (eGFP) fused at its carboxy terminus to the plasma membrane targeting motif of human K-Ras4B. The coding sequence of this protein designated eGFP-PM (previously known as GFP-tK;)[4] was inserted as an 870-bp Eco47III×XbaI restriction fragment into the polylinker of pLV.hCMV-IE.MCS.WHVoPRE after digestion of this plasmid with SmaI and XbaI. pLV.hCMV-IE.MCS.WHVoPRE is a derivative of pLV.hCMV-IE. IRES.eGFP.hHVBPRE, in which the DNA segment comprising the encephalomyocarditis virus internal ribosomal entry site (IRES), the eGFP open reading frame and the human hepatitis B virus posttranscriptional regulatory element (PRE) is replaced by the oPRE version of the woodchuck hepatitis virus PRE.[5] LV shuttle plasmids pLV.hCMV-IE.miniSOG-PM.hHBVPRE and pLV. hCMV-IE.eGFP-PM.WHVoPRE were subsequently used for the production of LV.miniSOG-PM and LV.eGFP-PM particles, respectively, using a previously described procedure. Restriction enzymes and other DNA modifying enzymes were obtained from New England Biolabs (Bioké,

Leiden, the Netherlands) or (Thermo Fisher Scientific, Bleiswijk, the Netherlands). Large-scale plasmid isolation was done with the JETSTAR 2.0 Plasmid Maxiprep kit (Genomed, Löhne, Germany) following the instructions of the manufacturer.

Culture and Genetic Modification/Lentiviral Transduction of NRVCs

SIN-LV suspensions stored in 100 µL portions at -80ºC were gradually thawed on ice prior use. At 4 day after culture initiation, NRVCs cultured on glass coverslips were transduced by adding SIN-LV suspension directly to culture medium. After 24 hours, the inoculum was removed and cells were washed once with phosphate-buffered saline (PBS) and 3 times with culture medium before fresh culture medium was given. Culture medium was refreshed daily for 2 additional days to establish high and stable expression level of eGFP-PM or miniSOG-PM in culture NRVCs. To determine the transduction efficiency, transduced cells were stained for nuclei by incubation them in culture medium containing Hoechst 33342 (Molecular Probes™, Thermo Fisher Scientific) at final concentration of 10 µg/mL. Then, cells were washed 3 times with PBS and later fixed with PBS containing 4% formaldehyde (Merck, Amsterdam, the Netherlands) for 15 min at room temperature (RT). After 3 times washing with PBS, coverslips were mounted in Vectashield mounting medium (Vector Laboratories, Burlingame, CA, USA). Finally, green fluorescent signals were assessed from the images acquired with a digital color camera-equipped fluorescence microscope (Nikon Eclipse 80i, Nikon Instruments Europe, Amstelveen, the Netherlands). For the experimental use, SIN-LVs were applied at doses that resulted in transduction of nearly 100% of NRVCs, without microscopic signs of cytotoxicity.

Immunocytology

To characterize our NRVC monolayer cultures, we performed immune fluorescent cell staining of non-transduced NRVCs cultured on glass coverslips. 3 days after plating, cells were fixed with PBS containing 4% formaldehyde (Merck) for 15 minutes at RT, washed 3 times with PBS and permeabilized by incubation for 10 minutes at RT with PBS containing 0.05% Triton-X100 (Sigma-Aldrich). Then wash 3 times with PBS containing 0.1% Tween-20 (Sigma-Aldrich). After washing, samples were incubated with primary antibodies diluted in PBS containing 10% fetal bovine serum (FBS; Sigma-Aldrich) and 1% bovine serum albumins (BSA; Sigma-Aldrich). Antibodies against the following antigens were used: sarcomeric α-actinin to detect cardiomyocytes (1:300; mouse IgG1, clone EA-53; Sigma-Aldrich) and collagen type 1 to identify fibroblastic cell types (1:300; rabbit IgG, polyclonal; Abcam, Cambridge, United Kingdom). After washing 3 times for 5 minutes with PBS containing 0.1% Tween-20, cells were incubated with appropriate Alexa Fluor© 488- or 568-conjugated secondary antibodies (1:500; Molecular Probes™, Thermo Fisher Scientific). Nuclear counterstaining was additionally performed by incubating the cells for 10 minutes at RT with 10 µg/mL Hoechst 33342. Coverslips were mounted in Vectashield mounting medium. Images were acquired with a digital color camera-equipped fluorescence microscope Nikon Eclipse 80i.

Reactive oxygen species (ROS) labeling

We performed live-cell imaging to detect ROS in native NRVCs (control), NRVCs expressing eGFP-PM (eGFP-PM-NRVCs) and NRVCs expressing miniSOG-PM (miniSOG-PM-NRVCs). To quantify the basic ROS level, CellROX© Deep Red reagent (Molecular Probes™, Thermo Fisher Scientific) was used to assess ROS under normal growth condition (37°C under 5% CO_2) in native NRVCs, eGFP-PM-NRVCs and miniSOG-PM-NRVCs, respectively. CellROX© Deep Red dye is cell-permeable and non-fluorescent in the reduced state; upon oxidation, it exhibits excitation/emission maxima at 640/665 nm. To stain the cells and nuclei, NRVCs were incubated under the normal growth conditions for 30 minutes with CellROX©Deep Red dye and Hoechst 33342 dye at a concentration of 5 μM/ml and 10μg/ml, respectively. Then, NRVCs were washed three times with pre-warm PBS before colorless culture medium was subsequently replaced. Immediately within 10 minutes, cells were imaged under the normal growth condition by Leica AF6000 LX inverted widefield microscopy system (Leica Microsystems B.V., Eindhoven, the Netherlands) equipped with a Hamamatsu EM-CCD camera through a HCX PL FLUOTAR L 40x/0.6 objective. Images were acquired using an A4 cube for Hoechst (excitation 360/40; emission 470/40), a YFP cube for eGFP/miniSOG (excitation 500/20; emission 535/30) and the DiD filter of a CYD fast filter wheel for ROS (excitation 625; emission 710). To minimize and prevent blue light to induce ROS overproduction during imaging, images acquired by a YFP cube were taken at the least of each acquisition per sample. To assess ROS level following blue-light (470 nM) illumination, 24-well plates containing native NRVCs, eGFP-PM-NRVCs, and miniSOG-PM-NRVCs were placed 0.5 cm above the blue-light source and illuminated for 4 minutes under the normal growth condition. Subsequently, cells were stained and imaged as described above. Here, the used light source is blue (470nm) LUXEON© rebel light emitting diode (LED), mounted on a 20 mm star CoolBase - 70 lm @ 700 mA (Quadica Developments Inc., Brantford, Ontario, Canada). The irradiance of 60 mW/mm^2 as measured after passing through culture plate and glass coverslip with a calibrated optical power meter PM100D conjugated with a S130C photodiode sensor (Thorlabs GmBH, Munich, Germany) was applied to activate ROS overproduction in this assay. Localization and quantification of fluorescence signals was done using dedicated software (Leica Application Suite [Leica Microsystems] and ImageJ [Rasband, W.S., National Institutes of Health, Bethesda, Maryland, USA])

Patch-clamp electrophysiological study

For patch-clamp recordings, NRVCs were transduced with either LV.miniSOG-PM or LV.eGFP-PM. 2-4 days after transducing, measurements were performed at 20-23°C. In brief, cells were transferred from culture medium to an external cellular solution containing (in mM): 126 NaCl, 11 glucose, 10 HEPES, 5.4 KCl, 1 $MgCl_2$, and 1.8 $CaCl_2$ (adjusted to pH 7.40 with NaOH). Approximately within 15-60 minutes after superfusion of external cellular solution, patch-clamp experiments were conducted. Only solitary cells observed beating were selected for the experiments to record electrical activities and membrane ionic currents. Signals were amplified and digitized using a conventional patch-clamp equipment consisting of a MultiClamp

700B amplifier and a Digidata 1440A A/D converter (Molecular Devices, Sunnyvale, CA, USA) connected to a personal computer. This patch-clamp equipment was controlled and driven by commercially available MultiClamp 700B Commander and Clampex v10.3 software (Molecular Devices) for Windows. Throughout experiments, the current and voltage outputs of amplifier were continuously sampled at intervals of 100 μs and recorded onto personal computer after low-pass filtered at 2-4 kHz with a four-pole Bessel filter. The patch pipettes were fabricated from borosilicate glass capillaries (1.5 mm outer diameter and 1.17 mm inner diameter, Harvard Apparatus, Kent, UK) with a vertical puller (P-30, Sutter Instruments, Novato, CA, USA). CPM-2 coating and polishing mircroforege (ALA Scientific Instruments, Farmingdale, NY, USA) was employed for fire-polishing to reshape and smooth pipette tips. For whole-cell experiments, pipettes had typical electrical resistances of 2-3 MW in the external cellular solution when filled with the internal solution containing (in mM): 80 potassium DL-aspartate, 40 KCl, 8 NaCl, 5.5 glucose, 5 HEPES, 5 EGTA, 1 $MgCl_2$, 4 Mg-ATP, and 0.1 Na_3-GTP (adjusted to pH 7.20 with KOH). The giga-ohm seal was formed by continuously applied 10-ms voltage steps from 0 to +5 mV at 10 Hz. After reaching giga-ohm seal, the holding potential was set to -50 mV, and the patch membrane was rupture by gentle suction applied to the pipette. [6] Whole-cell capacitance (C_m) was calculated from capacitive transient currents evoked during 5 mV steps from a holding potential of -50 mV and electrically removed with amplifier. To minimize voltage error and fetch the adequacy of the voltage-clamp, pipette series resistance was routinely monitored and electrically compensated by >75%. The estimated liquid-junction potential of 11 mV was corrected.

To activate ROS overproduction in NRVCs during patch-clamp experiments, blue light (470±20 nM, 0.3 mW/mm^2, measured after passing through all filters, optics and coverslips by a calibrated optical power meter PM100D conjugated with S130C photodiode sensor) delivery from a mercury arc lamp was served as light source for single-cell illumination. Activation blue light was coupled into an inverted microscope Zeiss Axiovert 35 (Carl Zeiss AG, Oberkochen, Germany) and modulated by shutter system (Lambda 10; Shutter Instruments).

Perforated patch-clamp technique was employed to record the electrical activities of transduced NRVCs before and after exposure to blue light. Pipette resistances between 4-5 MW were used for this techniques. Here, we adjusted our previously described procedures. [1] In brief, an ATP-, GTP and EGTA-free pipette solution containing (in mM): 80 potassium DL-aspartate, 40 KCl, 8 NaCl, 5.5 glucose, 5 HEPES, and 1 $MgCl_2$ (adjusted to pH 7.20 with KOH) was used to tip-fill patch pipettes, and the same pipette solution containing nystatin (120-200 μg/ml; Sigma-Aldrich) was used to back-fill the pipettes. After giga-ohm seal formation, the series resistance was monitored and shown progressively decline. Recordings were started after the series resistance had reached steady state of 15-10 MΩ stable (*i.e.* after 20-30 min). The integrity of the perforated patch was checked during and after recording for every experiment. We noted that the rupture of patch membrane abruptly increased capacitive current, unleashed the pipette solution to diffuse into the cells and caused an irreversible contracture because a specific chelator for calcium EGTA was absence. Therefore, we discarded those cells that showed sudden

appearance of the capacitive current or the irreversible contracture under the microscope to ensure reliability of recordings.

Optical-Voltage Mapping

Propagation of action potentials was investigated in monolayer cultures of NRVCs plated out onto 15-mm round glass coverslips in 24-well plates (Corning) at a cell density of $8x10^5$ cells per well. Three to four days of culture, the monolayers were transduced with lentiviral vectors encoding either miniSOG-PM or eGFP-PM. Between day 8 to day 9, cultures were optically mapped using voltage-sensitive dye di-4-ANEPPS (Molecular Probes™, Thermo Fisher Scientific) as described previously.[1,2] In brief, cultures without structural inhomogeneities as judged by light microscopy were selected for staining. Cultures were incubated with culture medium containing 8 µmol/L di-4-ANEPPS for under the normal growth condition for 10±5 minutes. Subsequently, pre-warm color less DMEM/HAMS F10 (Gibco™, Thermo Fisher Scientific) mixed in a 1:1 ratio medium (serum-free) were replaced the culture medium containing dry. Next, the electrical activities of monolayer cultures were examined at 37°C. Each mapping experiments normally did not exceed 30 minutes per 24-wells plate. Excitation light (e_{ex} = 525±25 nm) was delivered by a halogen arc-lamp (MHAB-150W, Moritex Corporation, San Jose, CA, USA) through epi-illumination. Fluorescent emission light passed through a dichroic mirror and a long-pass emission filter (>590 nm) and was focused onto a 100x100 pixels CMOS camera (Ultima-L, SciMedia, Costa Mesa, CA, USA) by a 1.6x converging lens (Leice, Wetzlar, Germany). This resulted in a spatial resolution of 160 µm/pixel and a field of view of 16 by 16 mm. Spontaneous or stimulated electrical activity was recorded for 6-24 seconds at 6ms exposure time per frame. Data analysis was performed with specialized software (Brainvision Analyze 1101, Brainvision Inc, Tokyo, Japan) after pixels signals were averaged with 8 of its nearest neighbors to minimize noise-artifacts. Conduction velocity (CV), maximal optical action potential upstroke (dF/dT_{max}), maximal action potential downstroke velocity (dF/dT_{min}), action potential duration until 30%, 50% and 80% repolarization ($APD_{30,\ 50\ and\ 80}$) were determined at ≤1 Hz at six different locations equally distributed throughout the culture and averaged before inclusion in further analyses. Spatial dispersion of repolarization was defined as the maximal difference in APD_{80} within a culture and was determined at activation frequencies of ≤1 Hz. 3D APD distribution maps, regional APD distribution histograms were plotted using custom Wolfram Mathematica software. In order to build activation maps, videos were equalized in oscillation amplitude per pixel, filtered with 3-pixel kernel Gauss 2d filter using custom ImageJ-based program. Then activation maps were built using standard Brainvision software.

Patterned illumination

Existing optical mapping setup was conjugated with computer-controlled digital micro-mirror device (DMD)-based, the Polygon 400, (P/N: DSI-G-000; Mightex Systems, Toronto, Ontario, Canada), to enable patterned illumination system (Supplementary Figure 3). 470-nm light from 3 watt high-power LED from LED source (LCS-0470-50-22; Mightex Systems) was projected

on DMD surface via liquid light guide (LLG-03-59-340-0800-1; Mighttex Systems). Reflection from DMD surface was projected and focused on the sample through a custom-built dichroic mirror (reflect 520-560 nm; pass >600 nm, Scimedia LtD, Costa Mesa, CA, USA) and an objective lens (1x). The constant 470-nm light intensity in the sample plane (0.3 mW/mm^2) was used in combination with various illumination time depending on experimental protocols. Light intensity was measured using S130C photodiode sensor by P100D optical power meter.

Data analysis and statistics

For off-line analysis, the data stored on personal computers were analyzed by pClamp V10.3 (Molecular Devices), BV analyze V13.12.20 (Brainvision Analyze 1101), and Graph Pad Prism software version 6 (GraphPad Software, Inc., La Jolla, CA). Unless otherwise stated, data were reported as mean ± standard error of mean (SEM). Statistical comparison of the same groups under control and experimental conditions was performed by both paired and unpaired Student's *t*-test. Statistical comparison of several groups to a control group was performed by oneway ANOVA followed by Turkey's post-test. Significant differences were determined at the P <0.05 level, unless specified. Statistical significance was expressed as follows: *: P<0.05, **: P<0.01, ***: P<0.001. The term *n* refers to the number of experiments.

Supplemental References

1. Engels MC, Askar SF, Jangsangthong W, Bingen BO, Feola I, Liu J, Majumder R, Versteegh MI, Braun J, Klautz RJ, Ypey DL, De Vries AA, Pijnappels DA. Forced fusion of human ventricular scar cells with cardiomyocytes suppresses arrhythmogenicity in a co-culture model. Cardiovasc Res. 2015; 107:601-12.
2. Askar SF, Ramkisoensing AA, Schalij MJ, Bingen BO, Swildens J, van der Laarse A, Atsma DE, de Vries AA, Ypey DL, Pijnappels DA. Antiproliferative treatment of myofibroblasts prevents arrhythmias in vitro by limiting myofibroblast-induced depolarization. Cardiovasc Res. 2011; 90:295-304.
3. Shu X, Lev-Ram V, Deerinck TJ, Qi Y, Ramko EB, Davidson MW, Jin Y, Ellisman MH, Tsien RY. A genetically encoded tag for correlated light and electron microscopy of intact cells, tissues, and organisms. PLoS Biol. 2011; 9:e1001041.
4. Apolloni A, Prior IA, Lindsay M, Parton RG, Hancock JF. H-ras but not K-ras traffics to the plasma membrane through the exocytic pathway. Mol Cell Biol. 2000; 20:2475-87.
5. Schambach A, Bohne J, Baum C, Hermann FG, Egerer L, von LD, Giroglou T. Woodchuck hepatitis virus post-transcriptional regulatory element deleted from X protein and promoter sequences enhances retroviral vector titer and expression. Gene Ther. 2006; 13:641-5.
6. Li C. A reliable whole cell clamp technique. Adv Physiol Educ. 2008; 32:209-11.

Supplemental Figures

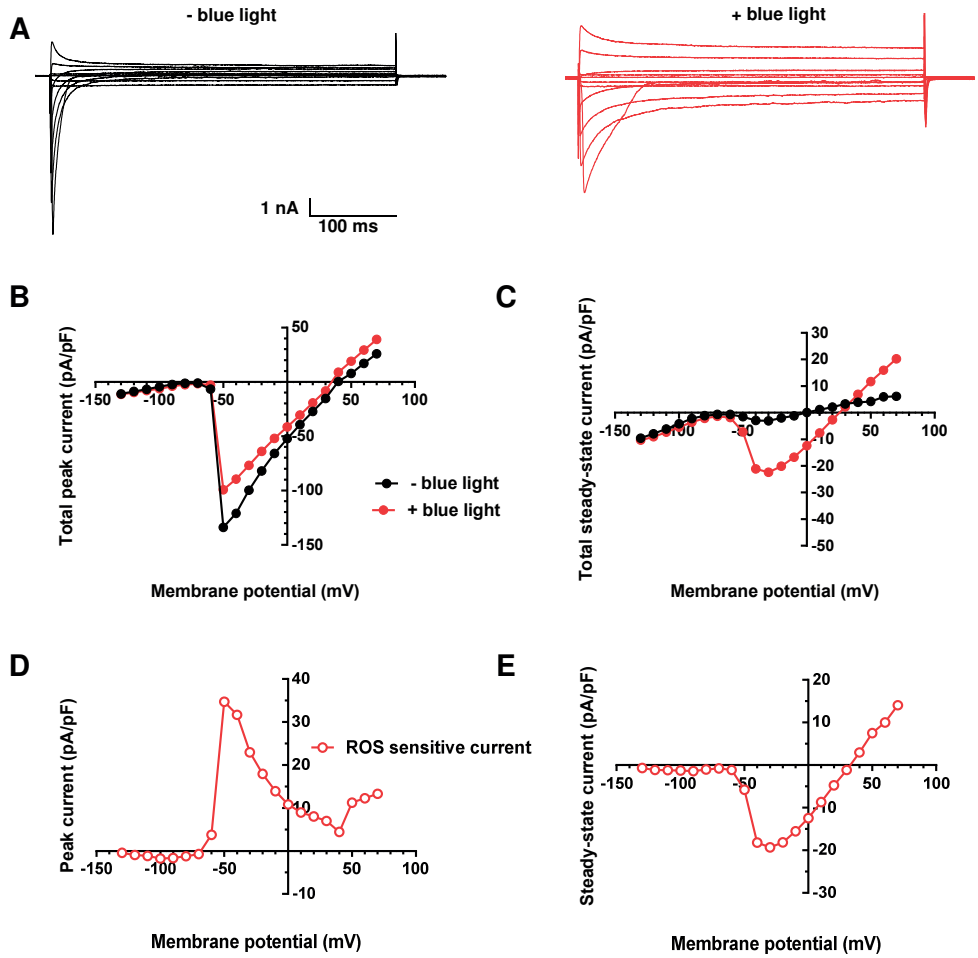

Supplementary Figure 1. Effects of ROS on total membrane currents of miniSOG-PM NRVC. The representative total membrane currents (A) of a miniSOG-PM-NRVC were obtained immediately after gaining the cell access (black trace) and after 10-s 470-nm-light illumination (red trace) by performing whole-cell voltage-clamp using 400-ms stepped pulses between -130 and +70 mV from a holding potential of -90 mV. The I-V relationships derived from (A) are shown in (B) for peak currents and C for steady-state currents. Filled black circles represent the control condition in the absence of 470-nm light. Filled red circles represent the OS condition when this cells was exposed to blue light for 10 s. The differences between the peak (D) and steady-state (E) currents before and after blue-light illumination are plotted against the membrane potential (open red circle). These I-V curves reveals ROS-sensitive current component, which is active upon exposure to blue light.

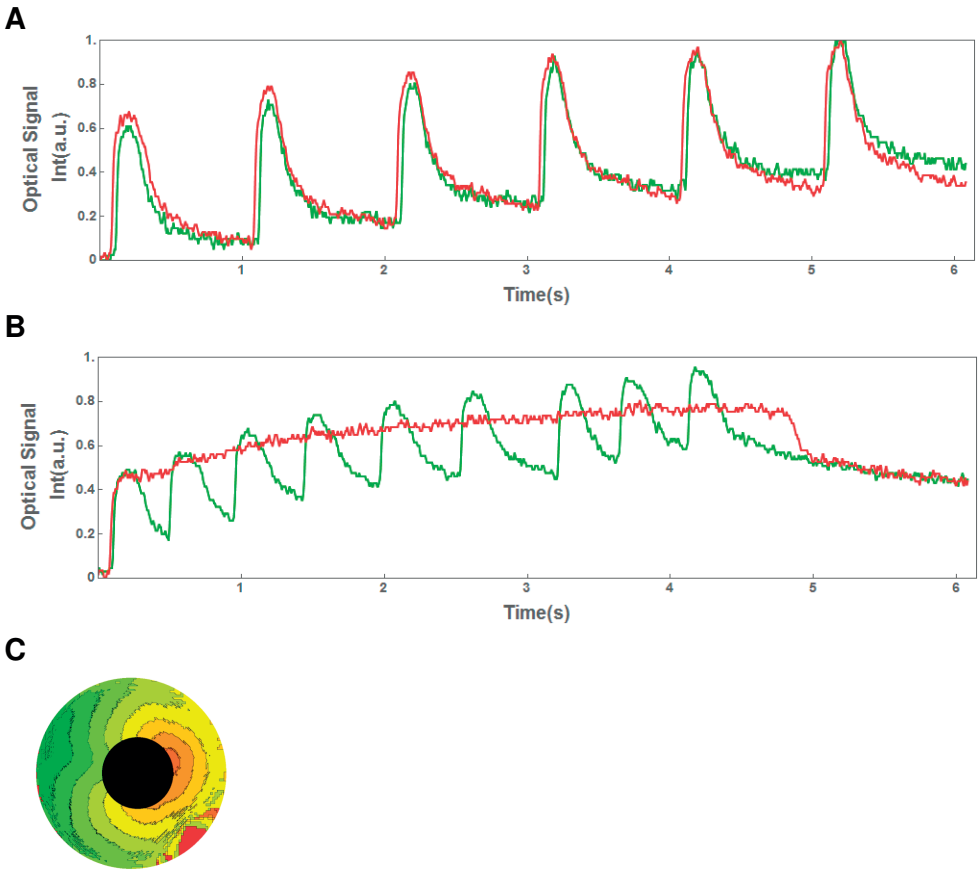

Supplementary Figure 2. Regional elevated ROS production disrupts calcium dynamics in miniSOG-PM-NRVC monolayers, leading to formation of quasistable calcium elevated level inside irradiated area and ectopic activity. A, Rhod2-AM optical-calcium traces during 1Hz electrical stimulation before irradiation shows baseline calcium dynamics. Red trace – central area, green trace – periphery area. B, Calcium transients were elicited by single electrical stimulus after illumination of the central area. Illuminated area (red trace) exhibits elevated calcium level lasting for 5 s. Ectopic activity (green trace) was initiated from the area of calcium elevation (OS zone). C, Typical example of ectopic beat propagation originated from OS zone.

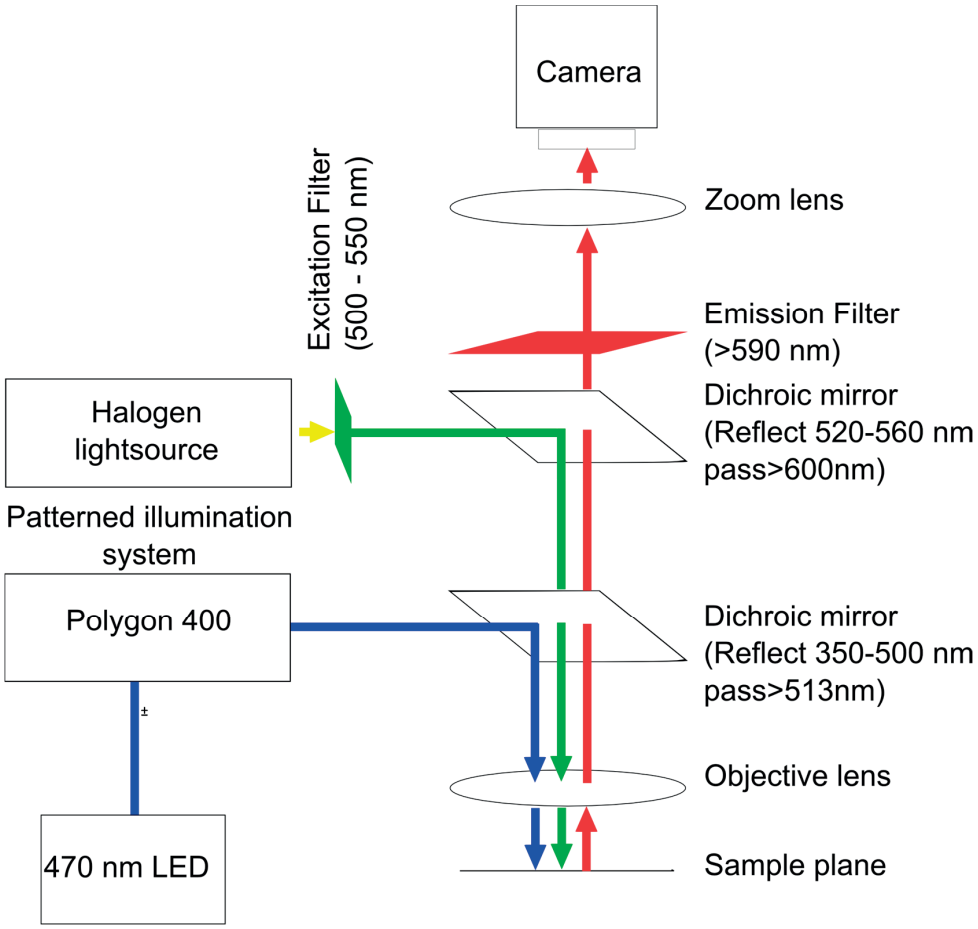

Supplementary Figure 3. Optical mapping and patterned illumination setup scheme. Experimental setup includes blue (470-nm) LED light source connected via light-guide to computer controlled DMD-based patterned illumination device (Polygon 400). Computer-generated patterns were projected on sample plane via reflection from dichroic mirror (513 nm pass) and focusing by objective lens. Halogen light source was bandpass filtered at 500-550 nm and dichroic mirrors for fluorescence excitation. Florescence signal went through emission filter (> 590 nm) to the camera.

Supplementary Table 1. Electrical physiological parameters in eGFP-PM upon 470-nm-light exposure. APD_{30}, APD_{50}, APD_{80} and CV inside (in) and outside (out) the irradiated area (6 mm ø) after 2 (n=10), 4 (n=10), and 6 (n=10) minutes upon 470-nm-light exposure. No significant differences were observed.

	2 minutes		4 minutes		6 minutes	
	out	**in**	**out**	**in**	**out**	**in**
APD (ms)	133±13	153±16	123±12	149±14	152±24	223±32
APD^{30} (ms)	170±17	190±21	148±16	177±17	188±30	260±28
APD^{50} (ms)	289±27	306±30	229±30	254±30	278±30	339±31
CV (^{80}cm/s)	18±0,7	19±0,8	18±0,9	18±1	19 ±0,5	19±0,4